Title

Atomic-Scale Imaging of Polymers and Precision Molecular Weight Analysis.

Authors

Marathianos, Arkadios

Magiakos, Alexandros

Han, Yisong

et al.

Publication Date

2024-12-04

DOI

10.1021/jacs.4c13812

Peer reviewed

JACS
JOURNAL OF THE AMERICAN CHEMICAL SOCIETY

pubs.acs.org/JACS
Communication

Atomic-Scale Imaging of Polymers and Precision Molecular Weight Analysis

Arkadios Marathianos, Alexandros Magiakos, Yisong Han, Ana Sanchez, Richard Whitfield, Jochen Kammerer, Athina Anastasaki, Paul Wilson, Joseph P. Patterson, Christopher Barner-Kowollik, and Evelina Liarou*

Cite This: J. Am. Chem. Soc. 2024, 146, 34292−34297
Read Online

ABSTRACT: Polymer design requires fine control over syntheses and a thorough understanding of their macromolecular structure. Herein, near-atomic level imaging of polymers is achieved, enabling the precise determination of one of the most important macromolecular characteristics: molecular weight. By judiciously designing and synthesizing different linear metal(loid)-rich homopolymers, subnanoscale polymer imaging is achieved through annular dark field-scanning transmission electron microscopy (ADF-STEM), owing to the incorporation of high Z atoms in the side chain of the monomeric units. The molecular weight of these polymers can be precisely determined by detecting and counting their metal(loid) atoms upon ADF-STEM imaging, at sample concentrations as low as 10 $\mu g \cdot mL^{-1}$. Notably, a commonly used C, H, and O-containing polymer (*i.e.*, poly(methyl acrylate)) that was thus far inaccessible at the atomic scale is derivatized to allow for subnano-level imaging, thus expanding the scope of our approach toward the atomic-level visualization of commodity polymers.

The design of soft matter with predefined properties necessitates the (sub)nanoscale analysis of polymers, tailored with precision for significant performance.[1,2] A fundamental characteristic of polymers is their molecular weight (MW). The leading techniques for MW determination are size exclusion chromatography (SEC), ^{1}H nuclear magnetic resonance (^{1}H NMR), and high-resolution mass spectrometry (HR-MS) (Scheme 1). Although well-established, these techniques possess significant limitations when complex systems are targeted, including organometallic[3,4] and conjugated polymers,[5,6] or complex architectures.[7,8] For instance, SEC requires the combination of suitable solvents, columns and MW standards,[9] ^{1}H NMR requires distinctive end-groups, while topologically complex polymers, with high dispersity and MW, are not suitable for HR-MS.[10,11]

Acknowledging those challenges, Junkers and colleagues developed a universal approach to determine polymer MW through diffusion-ordered NMR spectroscopy (DOSY), overcoming calibration and solvent implications,[12−14] while Haddleton and Lester developed a facile strategy for MW online monitoring through DOSY.[15,16] However, for polymers with compositional complexity and aggregation behavior in most solvents, solid-state MW analysis is necessary. Costantini and colleagues reported on the MW determination of conjugated polymers, through scanning tunnelling microscopy (STM) and vacuum electrospray deposition (ESD),[6] while another powerful example is the work from Matyjaszewski and Sheiko who achieved in-depth analysis of high MW cylindrical brushes using atomic force microscopy (AFM).[17−19] Although STM and AFM have provided valuable insights into the understanding of macromolecular characteristics, they are limited to the imaging of conjugated polymers or polymers with very high MW and branching.

Within the scope of visual understanding of polymers, electron microscopy (EM) techniques including (cryogenic) transmission electron microscopy, (Cryo-) TEM, and liquid-cell electron microscopy (LC-EM) have revolutionized the field of polymer imaging. Exemplary are the studies from Patterson,[1,20−26] Gianneschi,[27−33] Sommerdijk,[34,35] and de Jonge,[36−40] among others. However, the subnano level imaging of nonconjugated synthetic polymers has been largely inaccessible. Apart from their structural complexity, their elemental composition is mostly limited to C, O, H, and N, exhibiting similarity with most TEM support grids. Consequently, the low contrast obtained during conventional TEM does not allow for precise subnano level imaging. Additionally, their light element composition renders them challenging to detect through atomic-level EM methods, such as annular dark field (ADF) scanning transmission electron microscopy (STEM), where contrast depends on the atomic number.[1,41−44]

Our vision was to overcome those challenges and approach atomic-level analysis of polymers through ADF-STEM, as well as to visualize their MW (Scheme 1), by strategically designing the synthesis of metalloid-rich homopolymers bearing one arsenic (As) atom per monomer unit. For that purpose, free

Received: October 2, 2024
Revised: November 25, 2024
Accepted: November 26, 2024
Published: December 4, 2024

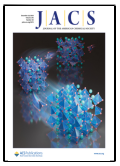

https://doi.org/10.1021/jacs.4c13812
J. Am. Chem. Soc. 2024, 146, 34292−34297

Scheme 1. Schematic Illustration of the Methods Traditionally Used to Determine the MW of Polymers and Our Approach through ADF-STEM

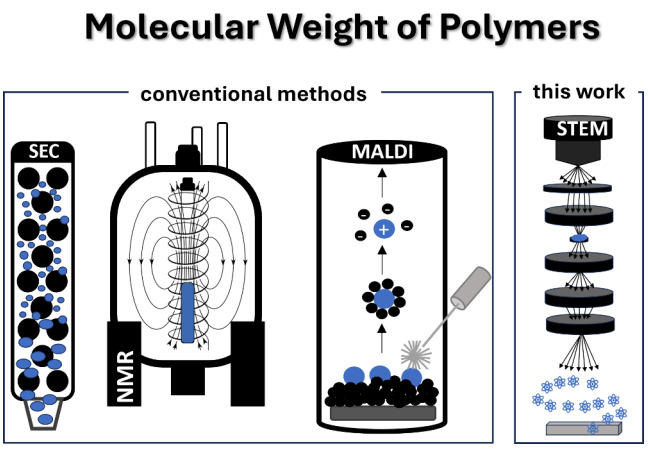

radical polymerization (FRP) and reversible deactivation radical polymerization (*i.e.*, reversible addition−fragmentation chain transfer polymerization, RAFT) were employed to generate polymers with various MW and $Đ$ values. To expand to another polymer family and metal functionality, ferrocenylmethyl methacrylate was used to generate an Fe-rich polymethacrylate. Finally, to render widely used polymers visible on the atomic level, a poly(methyl acrylate) (PMA) was derivatized with ferrocenecarboxylic acid, and its MW and $Đ$ were calculated through imaging.

Initially, an As-acrylamide monomer was synthesized according to the literature[45,46] and used to generate an As-polyacrylamide (PAsAm) through FRP ($PAsAm_{FRP}$, Figure S1, SI). A highly dilute (50 $\mu g \cdot mL^{-1}$ in 0.1 M NaOH) solution of the purified homopolymer was prepared and placed under vacuum prior to imaging (SI). To gain a first understanding of the As signal, we employed ADF-STEM through a double aberration corrected JEOL ARM200F microscope, operated at 200 kV. At 3 million times magnification (×3M), bright nanoclusters were evident (Figure S2), while at ×8M and ×12M magnification, their structure was elucidated, depicting the randomly coiled polymer chains consisting of As atoms (appearing as bright spots, Figure S2). To enhance sample stability and mitigate contamination, "beam shower" was applied prior to imaging at high magnifications.[47] Although the organic content is sensitive and prone to beam damage under the applied conditions,[46] the metalloid-rich chains remained intact throughout imaging. An advantage of this approach is that any potential damage to the organic components of the polymers by the electron beam will not affect the results of the MW analysis, as they depend only on the beam-stable metals.

Having achieved the detection of single chains and their As atoms, we sought to visualize the MW distribution of the polymers. Three well-defined PAsAms with targeted DP_n = 50, 20, and 10 were synthesized through RAFT polymerization (SI, Figures S3−S5), while aqueous-SEC and DOSY NMR were employed to determine the MW of the homopolymers after purification (Table 1).The ADF-STEM of $PAsAm_{50}$,

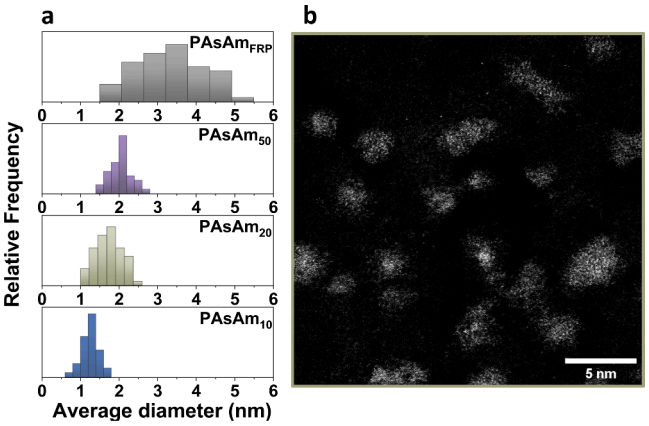

Figure 1. (a) Histograms showing the distribution of chain diameter for the four polymers and (b) high-resolution ADF-STEM image of $PAsAm_{20}$ (scale bar: 5 nm).

$PAsAm_{20}$ (Figure 1b), and $PAsAm_{10}$ at ×8M magnification revealed polymer chains smaller than in the case of $PAsAm_{FRP}$ (Figures 1a, 2c−f, and S6−S8). Owing to the different average chain length of the imaged polymers, the chain diameter increased with the increase in MW (Figure 1a), while the low $Đ$ polymers exhibited narrow diameter distribution, compared to $PAsAm_{FRP}$. Importantly, when the As-monomer was imaged under the same EM conditions, only individually scattered single As atoms were detected (Figure S9).

To determine the polymer MW and $Đ$, the intensities of single chains were calculated upon subtraction of their background, while the intensity of single As atoms was used as the calibrant, assuming a linear relationship between the integrated ADF intensity of single atoms and very small nanoclusters when kinematic diffraction effects dominate the signals collected by ADF-STEM imaging (Figure S10).[48−50] The same process was repeated for each sample individually in the same session. The integrated As atoms' intensity allowed

Table 1. Molecular Weight and $Đ$ Values from SEC, DOSY, and STEM for the Different Metal(loid)-rich Homopolymers

Polymer	$M_{n,SEC}$ [a]	$DP_{n,SEC}$ [a]	$M_{w,SEC}$ [a]	$Đ_{SEC}$ [a]	MW_{DOSY} [b]	$DP_{n,DOSY}$ [b]	MW_{STEM} [c]	$DP_{n,STEM}$ [c]	$Đ_{STEM}$ [c,d]
$PAsAm_{10}$	5,700	21	6,300	1.10	2,500	9	2,300	8	1.30
$PAsAm_{20}$	7,900	29	8,700	1.10	6,900	25	7,500	28	1.20
$PAsAm_{50}$	12,100	45	13,900	1.15	9,600	35	11,000	40	1.10
$PAsAm_{FRP}$	218,000	N/A	509,000	2.30	101,700	375	113,000[h]	417[h]	1.60
$PFerMMA_{10}$	5,900[e]	21[e]	8,600[e]	1.4[e,f]	3,700[g]	14[g]	3,500	13	1.40
	7,100[f]	25[f]	10,200[f]						

[a]Aqueous-SEC, average molecular weight values expressed as MW equivalents relative to PEG/PEO standards, [b]in D_2O/NaOH using an 80 MHz benchtop NMR, calculated through MaDDOSY,[15] [c]MW_{STEM} expressed in $g \cdot mol^{-1}$, conditions: 200 kV at ×8M magnification (and ×10M for $PAsAm_{10}$ and $PFerMMA_{10}$), [d]calculated based on the literature,[51] [e]$CHCl_3$-SEC, average molecular weight values expressed as MW equivalents to PS or [f]PMMA standards, [g]in $CDCl_3$ using an 80 MHz benchtop NMR, [h]average of the broad main distribution from 13,000 to 80,000 $g \cdot mol^{-1}$ (DP_n = 48−295) and chains reaching up to 240,000 $g \cdot mol^{-1}$ ($DP_n \sim 885$).

https://doi.org/10.1021/jacs.4c13812
J. Am. Chem. Soc. 2024, 146, 34292−34297

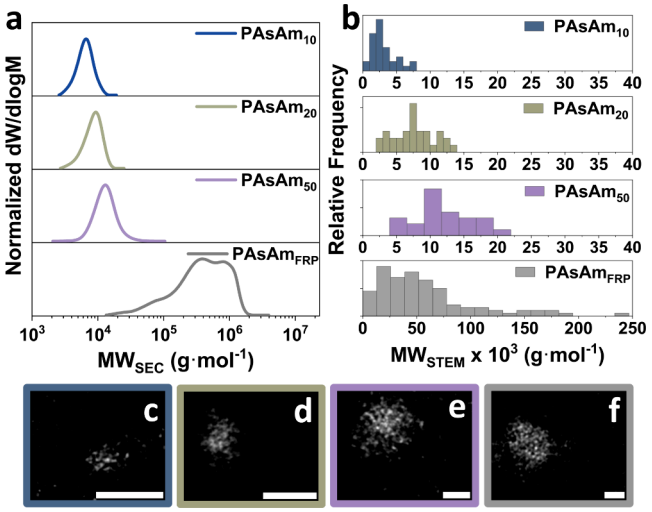

Figure 2. (a) Aqueous-SEC traces for $PAsAm_{10}$, $PAsAm_{20}$, $PAsAm_{50}$ and $PAsAm_{FRP}$. (b) MW_{STEM} distributions for the different polymers and ADF-STEM images showing segmented individual polymer chains for (c) $PAsAm_{10}$, (d) $PAsAm_{20}$, (e) $PAsAm_{50}$, and (f) $PAsAm_{FRP}$ (scale bars: 1 nm, *images were smoothed post imaging*).

for determination of the DP_n for $PAsAm_{50}$, $PAsAm_{20}$, and $PAsAm_{10}$ through atom counting (Table 1, SI).

In other words, the number of As atoms in each chain corresponded to DP_n, which was used to calculate the corresponding MW_{STEM}. The $Đ_{STEM}$ of the polymers was estimated according to the literature, based on standard deviation (σ), and the relation between $Đ$ and σ (SI).[51]

For the three well-defined polymers, MW_{STEM} was comparable with MW_{SEC}, while there was particularly good agreement between STEM and DOSY for $PAsAm_{10}$ and $PAsAm_{20}$ (Table 1; Figures 2a–b, S4, S5, S7, and S8). Importantly, in contrast with DOSY, STEM can provide a distribution of MW, representative of the nonidentical chain lengths in a synthetic polymer sample. For $PAsAm_{10}$, $M_{n,SEC}$ was significantly higher than MW_{DOSY} because low MWs necessitate better separation for higher accuracy. The $Đ_{STEM}$ results for $PAsAm_{20}$ and $PAsAm_{50}$ exhibited proximity to $Đ_{SEC}$ with both approaches resulting in $Đ_{STEM} \leq 1.2$.

To push the limits of our system, we attempted to calculate the MW_{STEM} of $PAsAm_{FRP}$. As expected, the STEM results showed a nonsymmetrical distribution of As atoms per chain, with a predominant broad MW_{STEM} distribution from 13,000 to ~80,000 g·mol^{-1}, along with the presence of high MW species up to ~240,000 g·mol^{-1}, with average MW_{STEM} = 113,000 g·mol^{-1} (Figure 2b, Table 1). The $Đ_{STEM}$ was 1.60, and although lower than the corresponding $Đ_{SEC}$, it illustrated the broad MW distribution of $PAsAm_{FRP}$. Samples with such high DP_n heterogeneity are highly challenging to quantitatively analyze with accuracy from single ADF-STEM images, since the very high MW chains might exhibit similarities with aggregated species; thus, careful interpretation of the images is necessary.[44,52] In general, highly pure polymer samples, careful sample preparation (*i.e.*, suitable support grids),[53,54] and thorough pretreatment (*i.e.*, vacuum drying, beam shower,[47,55] SI) are essential requirements, especially when sensitive samples are used.[53]

To expand the scope of metal functionality and polymer type, we synthesized an Fe-rich polymethacrylate (PFerMMA$_{10}$) (Figures 3a and S11, SI). As in the case of PAsAms, the

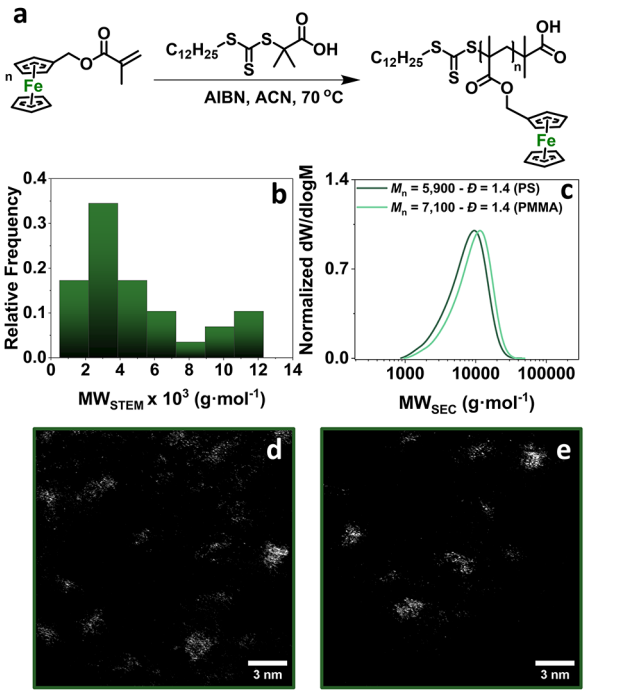

Figure 3. (a) Reaction scheme for the synthesis of $PFerMMA_{10}$, (b) MW_{STEM} histogram for $PFerMMA_{10}$, (c) SEC traces of $PFerMMA_{10}$, and (d and e) ADF-STEM images for $PFerMMA_{10}$ (scale bar: 3 nm).

MW_{STEM} (Figure 3b,d,e) was comparable to MW_{DOSY} while lower than $M_{n,SEC}$ (Table 1, Figure 3b,c). The SEC analysis of $PFerMMA_{10}$ exhibited distinct deviations when PMMA and PS standards were used (Figure 3c), highlighting the limitations of SEC when samples deviate from the calibrant. The range of MW_{STEM} (~1,000–12,000 g·mol^{-1}) with the existence of a second smaller population with MW ~9,500–12,000 g·mol^{-1}, was depicted in the obtained $Đ_{STEM}$ = 1.40 (Table 1). Therefore, the calculation of MW_{STEM} could be successfully achieved both for metalloid- and metal-containing acrylamide and methacrylate homopolymers, while their DP_n heterogeneity could be estimated through $Đ_{STEM}$ calculation.

Finally, we were interested in applying our approach to widely used C-, H-, and O-containing polymers, without using specially designed monomers. Thus, a PMA_{20} was synthesized (Figures 4a and S12, SI) and subsequently amidated using 4-amino-1-butanol, according to a literature procedure.[56] The amidation of PMA_{20} to poly(hydroxybutyl acrylamide, PHBAm) was quantitative, with a full shift of the PMA methyl protons as verified by ^{1}H NMR (Figure S14d), and full shift of the 1730 cm^{-1} peak (C=O, PMA) along with the formation of the 1635 cm^{-1} (C=O, amide) and 1543 cm^{-1} (N–H) PHBAm peaks, as verified by FT-IR (Figure S13). The shift toward higher MW was verified by THF-SEC (Figure 4b). The obtained –OH functional polymer was further functionalized through DCC/DMAP coupling with ferrocene (Fc) carboxylic acid (Figure 4a, SI), leading to derivatization of the parent PMA into an Fe-containing polyacrylamide. THF-SEC showed a clear shift toward higher MW (Figures 4b and S14); FT-IR verified the appearance of the C=O band (1700 cm^{-1}) attributed to the Fc-ester (Figure S13), while ^{1}H NMR confirmed the incorporation of the Fc moieties in the polymer (Figure S14d). ADF-STEM (Figure S15) revealed a predominant MW_{STEM} distribution at 3,000–4,300 g·mol^{-1}

https://doi.org/10.1021/jacs.4c13812
J. Am. Chem. Soc. 2024, 146, 34292–34297

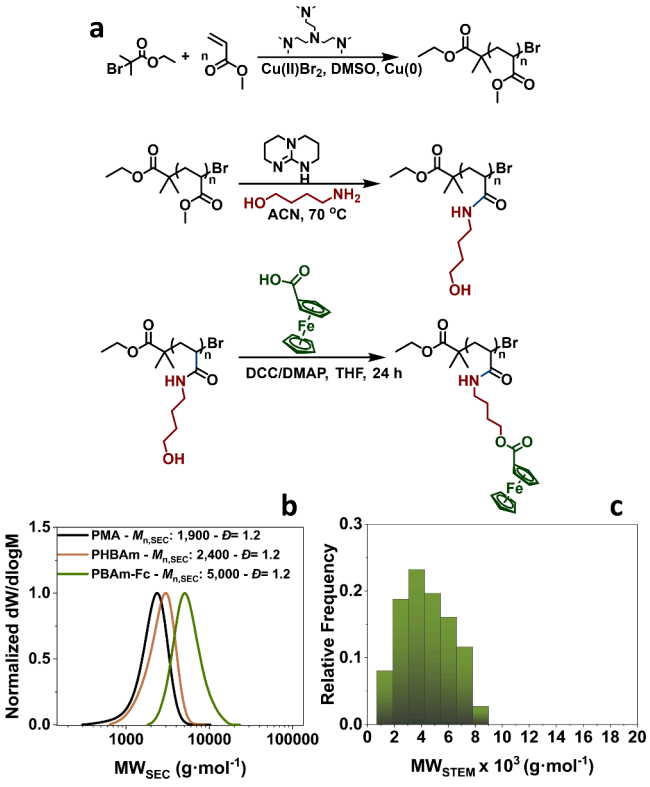

Figure 4. (a) Reaction scheme for the derivatization of PMA. (b) SEC traces of the parent PMA, the amidated derivative PHBAm, and the final PBAm-Fc, and (c) MW_{STEM} histogram of the functional PBAm-Fc.

(*vs* $M_{n,SEC}$ = 5,000, Figure 4b,c), indicating that on average ∼11 monomer units per chain had been functionalized (*vs* ∼14 from SEC). Therefore, the achievement of near-atomic level imaging of a commonly used polymer through derivatization has critical potential to serve as a promising strategy to visualize materials that had thus far been unobtainable. To the best of our knowledge, this is the first example of near-atomic level imaging of such a widely used polymer. Owing to the various synthetic tools available, we envisage that the modification of other commonly used polymers (*i.e.*, polystyrene, polyolefins) through different derivatization approaches (*i.e.*, Diels–Alder, click chemistry)[57−64] will expand the scope of this approach and establish it as a platform for advanced polymer imaging.

Our work presents the first approach toward atomic level imaging of synthetic polymers and MW determination through atom counting. By combining metal(loid)-containing monomers, different polymerization approaches, and atom counting through ADF-STEM, fundamental polymer characteristics were determined in the subnano scale. Additionally, the subnano level imaging of a widely used polymer (*i.e.*, PMA) was achieved upon derivatization. Our combinatorial approach sets the ground for atomic level analysis of polymer fundamentals that could not be imaged with such precision before and facilitates the profound understanding of their structure–property relationships.

■ ASSOCIATED CONTENT

Supporting Information

The Supporting Information is available free of charge at https://pubs.acs.org/doi/10.1021/jacs.4c13812.

Materials, instrumentation details, methods, synthetic procedures, NMR, SEC, FT-IR, UV–vis spectra, and ADF-STEM images (PDF)

■ AUTHOR INFORMATION

Corresponding Author

Evelina Liarou − *Department of Chemistry, University of Warwick, Coventry CV4 7AL, U.K.;* orcid.org/0000-0003-4491-5897; Email: Evelina.liarou.1@warwick.ac.uk

Authors

Arkadios Marathianos − *Polymer Characterization Research Technology Platform, University of Warwick, Coventry CV4 7AL, United Kingdom*

Alexandros Magiakos − *Department of Chemistry, University of Warwick, Coventry CV4 7AL, U.K.*

Yisong Han − *Department of Physics, University of Warwick, Coventry CV4 7AL, U.K.*

Ana Sanchez − *Department of Physics, University of Warwick, Coventry CV4 7AL, U.K.;* orcid.org/0000-0002-8230-6059

Richard Whitfield − *Laboratory of Polymeric Materials, Department of Materials, ETH Zurich, Zurich 8093, Switzerland;* orcid.org/0000-0003-4787-2060

Jochen Kammerer − *School of Chemistry and Physics, Centre for Materials Science, Queensland University of Technology (QUT), Brisbane City, QLD 4000, Australia*

Athina Anastasaki − *Laboratory of Polymeric Materials, Department of Materials, ETH Zurich, Zurich 8093, Switzerland;* orcid.org/0000-0002-6615-1026

Paul Wilson − *Department of Chemistry, University of Warwick, Coventry CV4 7AL, U.K.;* orcid.org/0000-0002-9760-899X

Joseph P. Patterson − *Department of Chemistry and Department of Materials Science and Engineering, University of California, Irvine, Irvine, California 92697-2025, United States;* orcid.org/0000-0002-1975-1854

Christopher Barner-Kowollik − *School of Chemistry and Physics, Centre for Materials Science, Queensland University of Technology (QUT), Brisbane City, QLD 4000, Australia; Institute of Nanotechnology, Karlsruhe Institute of Technology (KIT), 76131 Karlsruhe, Germany;* orcid.org/0000-0002-6745-0570

Complete contact information is available at: https://pubs.acs.org/10.1021/jacs.4c13812

Author Contributions

The manuscript was written through contributions of all authors. All authors have given approval to the final version of the manuscript.

Notes

The authors declare no competing financial interest.

■ ACKNOWLEDGMENTS

E.L. thanks the Leverhulme Trust, the Institute of Advanced Studies and the Eutopia Science and Innovation Fellowship for funding (ECF-2023-602 and European Union's Horizon 2020 research and innovation program under the Marie Skłodowska-Curie grant agreement No 945380), C.B.-K. acknowledges the Australian Research Council for a Laureate Fellowship and QUT's Centre for Materials Science for continued support; A.M. and P.W. are grateful for funding from Lubrizol and the

EPSRC for funding a PhD studentship (Prosperity Partnership, EP/V037943/1); P.W. also thanks the Royal Society and Tata companies (URF\R1\180274). The authors thank the Polymer RTP (UoW) for providing access to SEC and benchtop NMR, the Electron Microscopy RTP (UoW) for providing access to the microscopes, Dr Lijiang Song for access to the MS platform, Dr Ivan Prokes for access to the NMR equipment, and Dr Maria-Nefeli Antonopoulou and Dr Glen Jones for fruitful discussions on RAFT polymerization.

REFERENCES

(1) Dhaoui, R.; Cazarez, S. L.; Xing, L.; Baghdadi, E.; Mulvey, J. T.; Idris, N. S.; Hurst, P. J.; Vena, M. P.; Palma, G. D.; Patterson, J. P. 3D Visualization of Proteins within Metal-Organic Frameworks via Ferritin-Enabled Electron Microscopy. *Adv. Funct. Mater.* **2024**, *34* (13), 2312972.

(2) Pomerantseva, E.; Bonaccorso, F.; Feng, X.; Cui, Y.; Gogotsi, Y. Energy storage: The future enabled by nanomaterials. *Science* **2019**, *366* (6468), No. eaan8285.

(3) Zhang, J.; Wang, J.; Wei, C.; Wang, Y.; Xie, G.; Li, Y.; Li, M. Rapidly sequence-controlled electrosynthesis of organometallic polymers. *Nat. Commun.* **2020**, *11* (1), 2530.

(4) Meier, M. A. R.; Lohmeijer, B. G. G.; Schubert, U. S. Characterization of Defined Metal-Containing Supramolecular Block Copolymers. *Macromol. Rapid Commun.* **2003**, *24* (14), 852−857.

(5) Moro, S.; Siemons, N.; Drury, O.; Warr, D. A.; Moriarty, T. A.; Perdigão, L. M. A.; Pearce, D.; Moser, M.; Hallani, R. K.; Parker, J.; et al. The Effect of Glycol Side Chains on the Assembly and Microstructure of Conjugated Polymers. *ACS Nano* **2022**, *16* (12), 21303−21314.

(6) Moro, S.; Spencer, S. E. F.; Lester, D. W.; Nübling, F.; Sommer, M.; Costantini, G. Molecular-Scale Imaging Enables Direct Visualization of Molecular Defects and Chain Structure of Conjugated Polymers. *ACS Nano* **2024**, *18* (18), 11655−11664.

(7) Polymeropoulos, G.; Zapsas, G.; Ntetsikas, K.; Bilalis, P.; Gnanou, Y.; Hadjichristidis, N. 50th Anniversary Perspective: Polymers with Complex Architectures. *Macromolecules* **2017**, *50* (4), 1253−1290.

(8) Lutz, J.-F.; Lehn, J.-M.; Meijer, E. W.; Matyjaszewski, K. From precision polymers to complex materials and systems. *Nat. Rev. Mater.* **2016**, *1* (5), 16024.

(9) Barth, H. G.; Boyes, B. E.; Jackson, C. Size Exclusion Chromatography and Related Separation Techniques. *Anal. Chem.* **1998**, *70* (12), 251−278.

(10) Nakamura, S.; Fouquet, T.; Sato, H. Molecular Characterization of High Molecular Weight Polyesters by Matrix-Assisted Laser Desorption/Ionization High-Resolution Time-of-Flight Mass Spectrometry Combined with On-plate Alkaline Degradation and Mass Defect Analysis. *J. Am. Soc. Mass. Spectrom.* **2019**, *30* (2), 355−367.

(11) Steinkoenig, J.; Rothfuss, H.; Lauer, A.; Tuten, B. T.; Barner-Kowollik, C. Imaging Single-Chain Nanoparticle Folding via High-Resolution Mass Spectrometry. *J. Am. Chem. Soc.* **2017**, *139* (1), 51−54.

(12) Voorter, P.-J.; McKay, A.; Dai, J.; Paravagna, O.; Cameron, N. R.; Junkers, T. Solvent-Independent Molecular Weight Determination of Polymers Based on a Truly Universal Calibration. *Angew. Chem., Int. Ed.* **2022**, *61* (5), No. e202114536.

(13) Silva, I. W. F.; McKay, A.; Sokolova, A.; Junkers, T. Towards the universal use of DOSY as a molar mass characterization tool: temperature dependence investigations and a software tool to process diffusion coefficients. *Polym. Chem.* **2024**, *15* (13), 1303−1309.

(14) Voorter, P.-J.; Wagner, M.; Rosenauer, C.; Dai, J.; Subramanian, P.; McKay, A.; Cameron, N. R.; Michels, J. J.; Junkers, T. A fast and efficient way of obtaining the average molecular weight of block copolymers via DOSY. *Polym. Chem.* **2023**, *14* (46), 5140−5146.

(15) Tooley, O.; Pointer, W.; Radmall, R.; Hall, M.; Beyer, V.; Stakem, K.; Swift, T.; Town, J.; Junkers, T.; Wilson, P.; et al. MaDDOSY (Mass Determination Diffusion Ordered Spectroscopy) using an 80 MHz Bench Top NMR for the Rapid Determination of Polymer and Macromolecular Molecular Weight. *Macromol. Rapid Commun.* **2024**, *45* (8), 2300692.

(16) Tooley, O.; Pointer, W.; Radmall, R.; Hall, M.; Swift, T.; Town, J.; Aydogan, C.; Junkers, T.; Wilson, P.; Lester, D.; et al. Real-Time Determination of Molecular Weight: Use of MaDDOSY (Mass Determination Diffusion Ordered Spectroscopy) to Monitor the Progress of Polymerization Reactions. *ACS Polym. Au* **2024**, *4* (4), 311−319.

(17) Sheiko, S. S.; da Silva, M.; Shirvaniants, D.; LaRue, I.; Prokhorova, S.; Moeller, M.; Beers, K.; Matyjaszewski, K. Measuring Molecular Weight by Atomic Force Microscopy. *J. Am. Chem. Soc.* **2003**, *125* (22), 6725−6728.

(18) Sheiko, S. S.; Möller, M. Visualization of MacromoleculesA First Step to Manipulation and Controlled Response. *Chem. Rev.* **2001**, *101* (12), 4099−4124.

(19) Yu-Su, S. Y.; Sun, F. C.; Sheiko, S. S.; Konkolewicz, D.; Lee, H.-i.; Matyjaszewski, K. Molecular Imaging and Analysis of Branching Topology in Polyacrylates by Atomic Force Microscopy. *Macromolecules* **2011**, *44* (15), 5928−5936.

(20) Gibson, W.; Mulvey, J. T.; Das, S.; Selmani, S.; Merham, J. G.; Rakowski, A. M.; Schwartz, E.; Hochbaum, A. I.; Guan, Z.; Green, J. R.; et al. Observing the Dynamics of an Electrochemically Driven Active Material with Liquid Electron Microscopy. *ACS Nano* **2024**, *18* (18), 11898−11909.

(21) Hurst, P. J.; Graham, A. A.; Patterson, J. P. Gaining Structural Control by Modification of Polymerization Rate in Ring-Opening Polymerization-Induced Crystallization-Driven Self-Assembly. *ACS Polym. Au* **2022**, *2* (6), 501−509.

(22) Kunnas, P.; de Jonge, N.; Patterson, J. P. The effect of nanochannel length on in situ loading times of diffusion-propelled nanoparticles in liquid cell electron microscopy. *Ultramicroscopy* **2024**, *255*, 113865.

(23) Mulvey, J. T.; Rizvi, A.; Patterson, J. P. Liquid Electron Microscopy with Non-Aqueous Solvents: Evaluating the Beam-Sample Interactions of Complex Liquid Structures. *Microsc. Microanal.* **2023**, *29* (Supplement_1), 1758−1760.

(24) Rizvi, A.; Mulvey, J. T.; Carpenter, B. P.; Talosig, R.; Patterson, J. P. A Close Look at Molecular Self-Assembly with the Transmission Electron Microscope. *Chem. Rev.* **2021**, *121* (22), 14232−14280.

(25) Rizvi, A.; Mulvey, J. T.; Patterson, J. P. Observation of Liquid-Liquid-Phase Separation and Vesicle Spreading during Supported Bilayer Formation via Liquid-Phase Transmission Electron Microscopy. *Nano Lett.* **2021**, *21* (24), 10325−10332.

(26) Rizvi, A.; Patterson, J. P. Liquid-liquid phase separation induced auto-confinement. *Soft Matter* **2024**, *20* (9), 1978−1982.

(27) Korpanty, J.; Gianneschi, N. C. Exploration of Organic Nanomaterials with Liquid-Phase Transmission Electron Microscopy. *Acc. Chem. Res.* **2023**, *56* (17), 2298−2312.

(28) Korpanty, J.; Gnanasekaran, K.; Venkatramani, C.; Zang, N.; Gianneschi, N. C. Organic solution-phase transmission electron microscopy of copolymer nanoassembly morphology and dynamics. *Cell Rep. Phys. Sci.* **2022**, *3* (3), 100772.

(29) Korpanty, J.; Parent, L. R.; Hampu, N.; Weigand, S.; Gianneschi, N. C. Thermoresponsive polymer assemblies via variable temperature liquid-phase transmission electron microscopy and small angle X-ray scattering. *Nat. Commun.* **2021**, *12* (1), 6568.

(30) Korpanty, J.; Wang, C.; Gianneschi, N. C. Upper critical solution temperature polymer assemblies via variable temperature liquid phase transmission electron microscopy and liquid resonant soft X-ray scattering. *Nat. Commun.* **2023**, *14* (1), 3441.

(31) Scheutz, G. M.; Touve, M. A.; Carlini, A. S.; Garrison, J. B.; Gnanasekaran, K.; Sumerlin, B. S.; Gianneschi, N. C. Probing Thermoresponsive Polymerization-Induced Self-Assembly with Variable-Temperature Liquid-Cell Transmission Electron Microscopy. *Matter* **2021**, *4* (2), 722−736.

(32) Parent, L. R.; Vratsanos, M.; Jin, B.; De Yoreo, J. J.; Gianneschi, N. C. Chemical and physical transformations of carbon-based

https://doi.org/10.1021/jacs.4c13812
J. Am. Chem. Soc. 2024, 146, 34292−34297

nanomaterials observed by liquid phase transmission electron microscopy. *MRS Bull.* **2020**, *45* (9), 727−737.
(33) Parent, L. R.; Gnanasekaran, K.; Korpanty, J.; Gianneschi, N. C. 100th Anniversary of Macromolecular Science Viewpoint: Polymeric Materials by In Situ Liquid-Phase Transmission Electron Microscopy. *ACS Macro Lett.* **2021**, *10* (1), 14−38.
(34) Rutten, L.; de Beer, M.; Roverts, R.; Sánchez, E. M.; Sommerdijk, N. A Cryo-/Liquid Phase Correlative Light Electron Microscopy Workflow to Visualize Crystallization Processes in Graphene Liquid Cells. *Microsc. Microanal.* **2023**, *29* (Supplement_1), 1935−1936.
(35) Xu, Y.; Tijssen, K. C. H.; Bomans, P. H. H.; Akiva, A.; Friedrich, H.; Kentgens, A. P. M.; Sommerdijk, N. A. J. M. Microscopic structure of the polymer-induced liquid precursor for calcium carbonate. *Nat. Commun.* **2018**, *9* (1), 2582.
(36) Kunnas, P.; Moradi, M.-A.; Sommerdijk, N.; de Jonge, N. Strategy for optimizing experimental settings for studying low atomic number colloidal assemblies using liquid phase scanning transmission electron microscopy. *Ultramicroscopy* **2022**, *240*, 113596.
(37) Ross, F. M.; Wang, C.; de Jonge, N. Transmission electron microscopy of specimens and processes in liquids. *MRS Bull.* **2016**, *41* (10), 791−803.
(38) Wu, H.; Friedrich, H.; Patterson, J. P.; Sommerdijk, N. A. J. M.; de Jonge, N. Liquid-Phase Electron Microscopy for Soft Matter Science and Biology. *Adv. Mater.* **2020**, *32* (25), 2001582.
(39) Textor, M.; de Jonge, N. Strategies for Preparing Graphene Liquid Cells for Transmission Electron Microscopy. *Nano Lett.* **2018**, *18* (6), 3313−3321.
(40) de Jonge, N.; Ross, F. M. Electron microscopy of specimens in liquid. *Nat. Nanotechnol.* **2011**, *6* (11), 695−704.
(41) Kübel, C.; Voigt, A.; Schoenmakers, R.; Otten, M.; Su, D.; Lee, T.-C.; Carlsson, A.; Bradley, J. Recent Advances in Electron Tomography: TEM and HAADF-STEM Tomography for Materials Science and Semiconductor Applications. *Microsc. Microanal.* **2005**, *11* (5), 378−400.
(42) Sohlberg, K.; Pennycook, T. J.; Zhou, W.; Pennycook, S. J. Insights into the physical chemistry of materials from advances in HAADF-STEM. *Phys. Chem. Chem. Phys.* **2015**, *17* (6), 3982−4006.
(43) Loos, J.; Sourty, E.; Lu, K.; de With, G.; v. Bavel, S. Imaging Polymer Systems with High-Angle Annular Dark Field Scanning Transmission Electron Microscopy (HAADF-STEM). *Macromolecules* **2009**, *42* (7), 2581−2586.
(44) De Backer, A.; Bals, S.; Van Aert, S. A decade of atom-counting in STEM: From the first results toward reliable 3D atomic models from a single projection. *Ultramicroscopy* **2023**, *247*, 113702.
(45) Footman, C.; de Jongh, P. A. J. M.; Tanaka, J.; Peltier, R.; Kempe, K.; Davis, T. P.; Wilson, P. Thiol-reactive (co)polymer scaffolds comprising organic arsenical acrylamides. *Chem. Commun.* **2017**, *53* (60), 8447−8450.
(46) Wilson, P.; Anastasaki, A.; Owen, M. R.; Kempe, K.; Haddleton, D. M.; Mann, S. K.; Johnston, A. P. R.; Quinn, J. F.; Whittaker, M. R.; Hogg, P. J.; et al. Organic Arsenicals As Efficient and Highly Specific Linkers for Protein/Peptide-Polymer Conjugation. *J. Am. Chem. Soc.* **2015**, *137* (12), 4215−4222.
(47) Ramachandra, R.; Demers, H.; de Jonge, N. Atomic-resolution scanning transmission electron microscopy through 50-nm-thick silicon nitride membranes. *Appl. Phys. Lett.* **2011**, *98* (9), 93109.
(48) Han, Y.; He, D. S.; Liu, Y.; Xie, S.; Tsukuda, T.; Li, Z. Y. Size and Shape of Nanoclusters: Single-Shot Imaging Approach. *Small* **2012**, *8* (15), 2361−2364 (acccessed 2024/07/10).
(49) Wang, Z. W.; Palmer, R. E. Mass Spectrometry and Dynamics of Gold Adatoms Observed on the Surface of Size-Selected Au Nanoclusters. *Nano Lett.* **2012**, *12* (1), 91−95.
(50) Han, Y.; He, D. S.; Li, Z. Y. Direct observation of dynamic events of Au clusters on MgO(100) by HAADF-STEM. *J. Nanopart. Res.* **2013**, *15* (9), 1941.
(51) Harrisson, S. The downside of dispersity: why the standard deviation is a better measure of dispersion in precision polymerization. *Polym. Chem.* **2018**, *9* (12), 1366−1370.
(52) Şentürk, D. G.; Yu, C. P.; De Backer, A.; Van Aert, S. Atom counting from a combination of two ADF STEM images. *Ultramicroscopy* **2024**, *255*, 113859.
(53) Patterson, J. P.; Sanchez, A. M.; Petzetakis, N.; Smart, T. P.; Epps, T. H., III; Portman, I.; Wilson, N. R.; O'Reilly, R. K. A simple approach to characterizing block copolymer assemblies: graphene oxide supports for high contrast multi-technique imaging. *Soft Matter* **2012**, *8* (12), 3322−3328.
(54) Pantelic, R. S.; Meyer, J. C.; Kaiser, U.; Stahlberg, H. The application of graphene as a sample support in transmission electron microscopy. *Solid State Commun.* **2012**, *152* (15), 1375−1382.
(55) Egerton, R. F.; Li, P.; Malac, M. Radiation damage in the TEM and SEM. *Micron* **2004**, *35* (6), 399−409.
(56) Van Guyse, J. F. R.; Verjans, J.; Vandewalle, S.; De Bruycker, K.; Du Prez, F. E.; Hoogenboom, R. Full and Partial Amidation of Poly(methyl acrylate) as Basis for Functional Polyacrylamide (Co)Polymers. *Macromolecules* **2019**, *52* (14), 5102−5109.
(57) Easterling, C. P.; Kubo, T.; Orr, Z. M.; Fanucci, G. E.; Sumerlin, B. S. Synthetic upcycling of polyacrylates through organocatalyzed post-polymerization modification. *Chem. Sci.* **2017**, *8* (11), 7705−7709.
(58) Fleischmann, C.; Anastasaki, A.; Gutekunst, W. R.; McGrath, A. J.; Hustad, P. D.; Clark, P. G.; Laitar, D. S.; Hawker, C. J. Direct access to functional (Meth) acrylate copolymers through transesterification with lithium alkoxides. *J. Polym. Sci., Part A: Polym. Chem.* **2017**, *55* (9), 1566−1574.
(59) Hoyle, C. E.; Bowman, C. N. Thiol-Ene Click Chemistry. *Angew. Chem., Int. Ed.* **2010**, *49* (9), 1540−1573.
(60) Billiet, S.; De Bruycker, K.; Driessen, F.; Goossens, H.; Van Speybroeck, V.; Winne, J. M.; Du Prez, F. E. Triazolinediones enable ultrafast and reversible click chemistry for the design of dynamic polymer systems. *Nat. Chem.* **2014**, *6* (9), 815−821.
(61) Liarou, E.; Houck, H. A.; Du Prez, F. E. Reversible Transformations of Polymer Topologies through Visible Light and Darkness. *J. Am. Chem. Soc.* **2022**, *144* (15), 6954−6963.
(62) Sun, H.; Kabb, C. P.; Dai, Y.; Hill, M. R.; Ghiviriga, I.; Bapat, A. P.; Sumerlin, B. S. Macromolecular metamorphosis via stimulus-induced transformations of polymer architecture. *Nat. Chem.* **2017**, *9* (8), 817−823.
(63) Ogura, Y.; Terashima, T.; Sawamoto, M. Terminal-Selective Transesterification of Chlorine-Capped Poly(Methyl Methacrylate)s: A Modular Approach to Telechelic and Pinpoint-Functionalized Polymers. *J. Am. Chem. Soc.* **2016**, *138* (15), 5012−5015.
(64) Kakuchi, R.; Wongsanoh, K.; Hoven, V. P.; Theato, P. Activation of stable polymeric esters by using organo-activated acyl transfer reactions. *J. Polym. Sci., Part A: Polym. Chem.* **2014**, *52* (9), 1353−1358.

https://doi.org/10.1021/jacs.4c13812
J. Am. Chem. Soc. 2024, 146, 34292−34297